

**Supplementary Material:
BSE@GW-Based Protocol for Spin-Vibronic
Quantum Dynamics Using the Linear Vibronic
Coupling Model. Formulation and Application
to an Fe(II) Compound**

Florian Bogdain,[†] Sebastian Mai,[‡] Leticia González,[¶] and Oliver Kühn^{*,†}

[†]*Institute of Physics, University of Rostock, Albert-Einstein-Str. 23-24, D-18059, Rostock,
Germany*

[‡]*Institute of Theoretical Chemistry, Faculty of Chemistry, University of Vienna,
Währinger Straße 17, 1090 Wien, Austria*

[¶]*Vienna Research Platform on Accelerating Photoreaction Discovery, University of
Vienna, Währinger Straße 17, 1090 Vienna, Austria*

E-mail: oliver.kuehn@uni-rostock.de

Contents

S1: Choice of Basis Set

S2: Validity of LVC Model

S3: Structure of the ML-Trees

S4: Adjacency Matrix of Model (IV)

S5: Population Dynamics for Larger Convergence Threshold

S6: 42-dimensional Model

S7: Discussion of Accuracy of State Couplings

S8: Dependence on the Used XC-Functional

S9: Excitation Spectra

S1 Choice of Basis Set

In general, the BSE@GW framework appears to be much more susceptible to changes in the basis set than TD-DFT. Figure S1 shows the rather large differences a different basis set can cause. The first case uses a def2-SVP basis set for the ligand structure and a def2-TZVP for the central metal. The second calculation relied only on the def2-TZVP basis set for all atoms (as in main text).

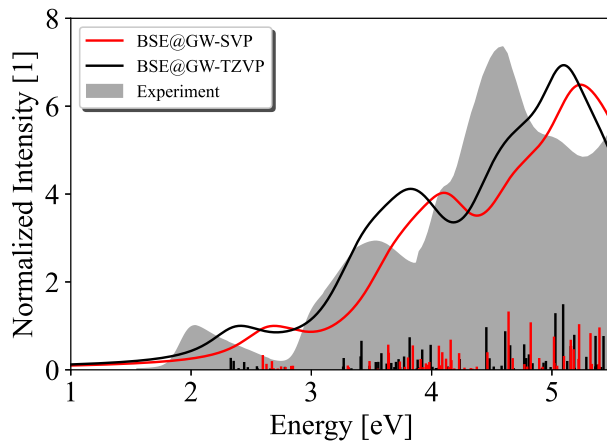


Figure S1: UV-vis spectra calculated using two different basis sets

S2 Validity of LVC Model

The quality of the LVC model was tested for several normal modes across the entire frequency range and are depicted in Figure S2. Close to the equilibrium geometry we observe a decent alignment of the LVC model with the true PES. Larger deviations are only observed in the area where the PES show a strong anharmonic character or if the coupling between states becomes very strong, up to the point where the linear approximation is no longer valid.

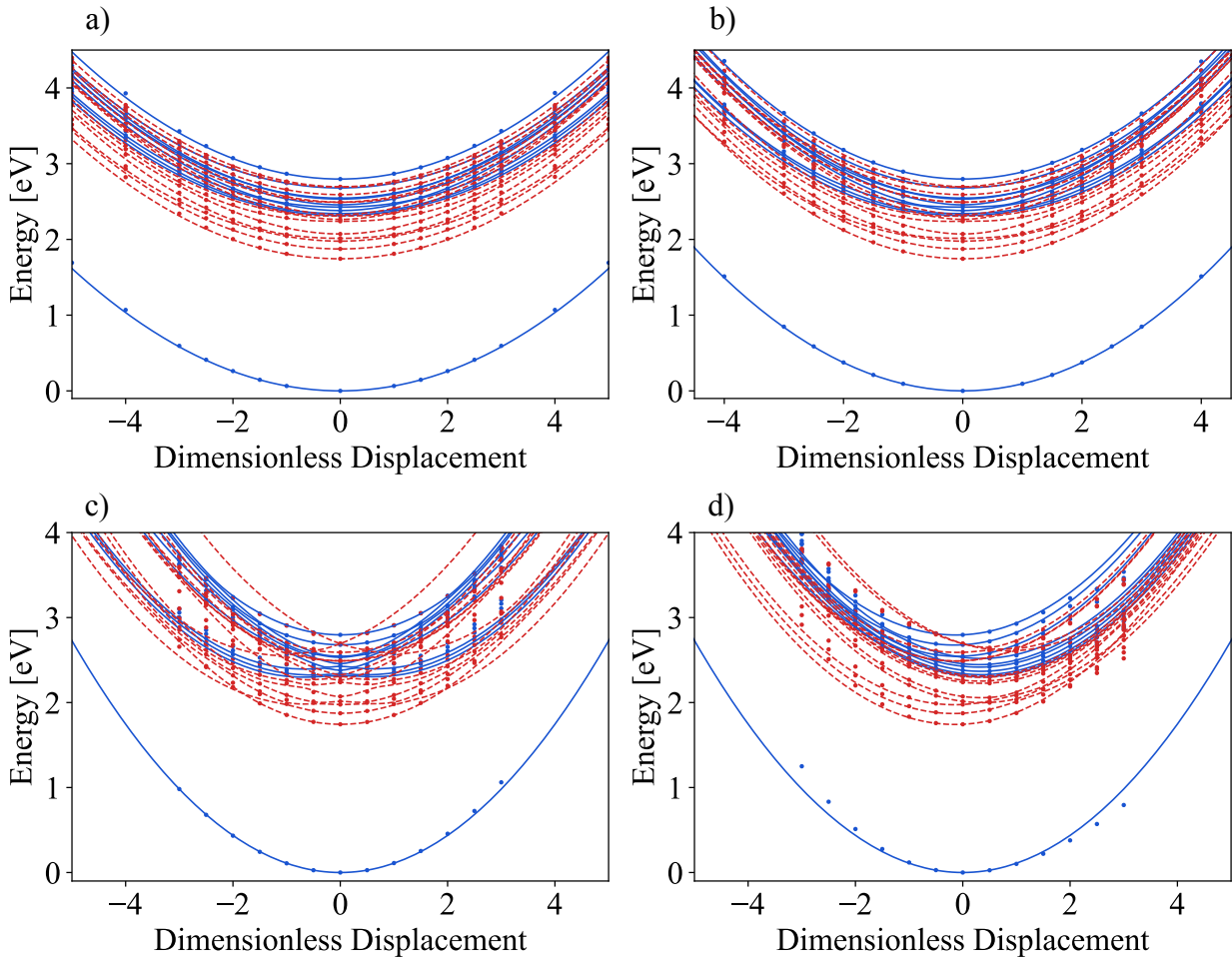


Figure S2: Adiabatic PES for normal modes a) 118 (1045 cm^{-1}), b) 173 (150 cm^{-1}), c) 190 (1761 cm^{-1}), and d) 191 (1762 cm^{-1}). Dots correspond to single point calculations, solid curves LVC model. Continuous blue lines are used to indicate singlet states, whereas dashed red lines are used for triplet states.

S3 Structure of the ML-Trees

All trees were generated such that the convergence threshold reached 1% for p_{NO} at each node. The only exception is figure S7, which depicts the fully converged ML-tree for model (IV).

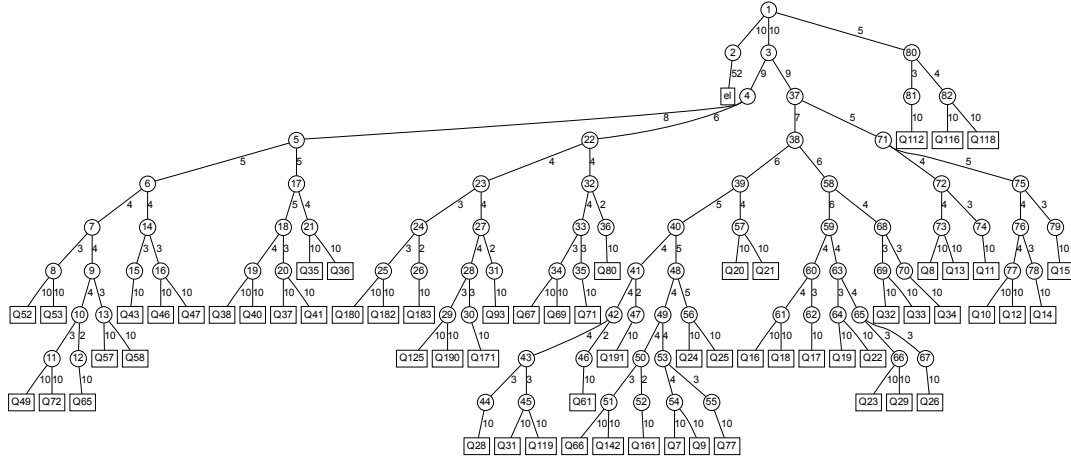


Figure S3: ML-tree for model (I).

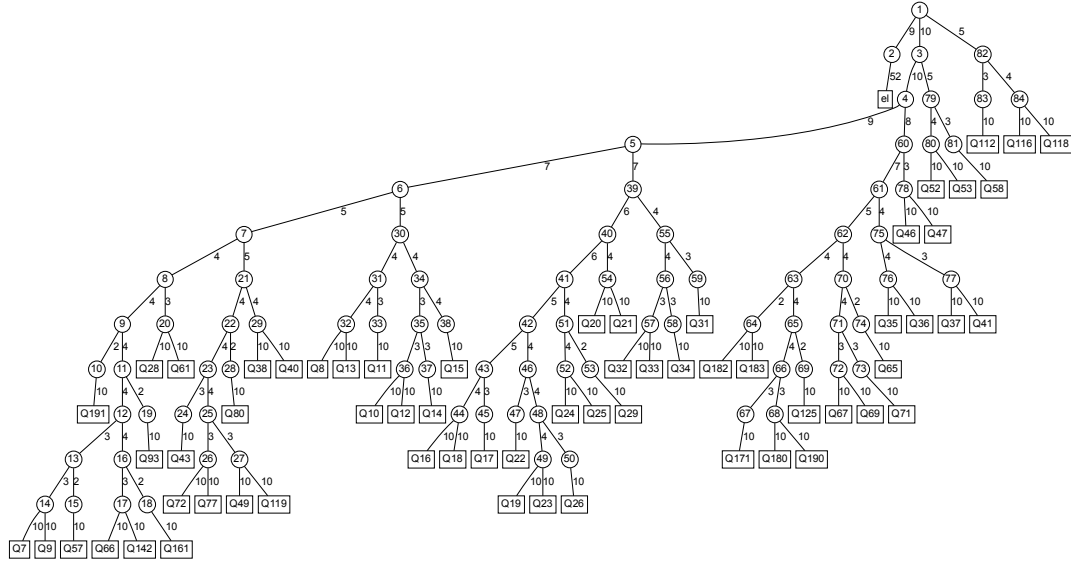


Figure S4: ML-tree for model (II).

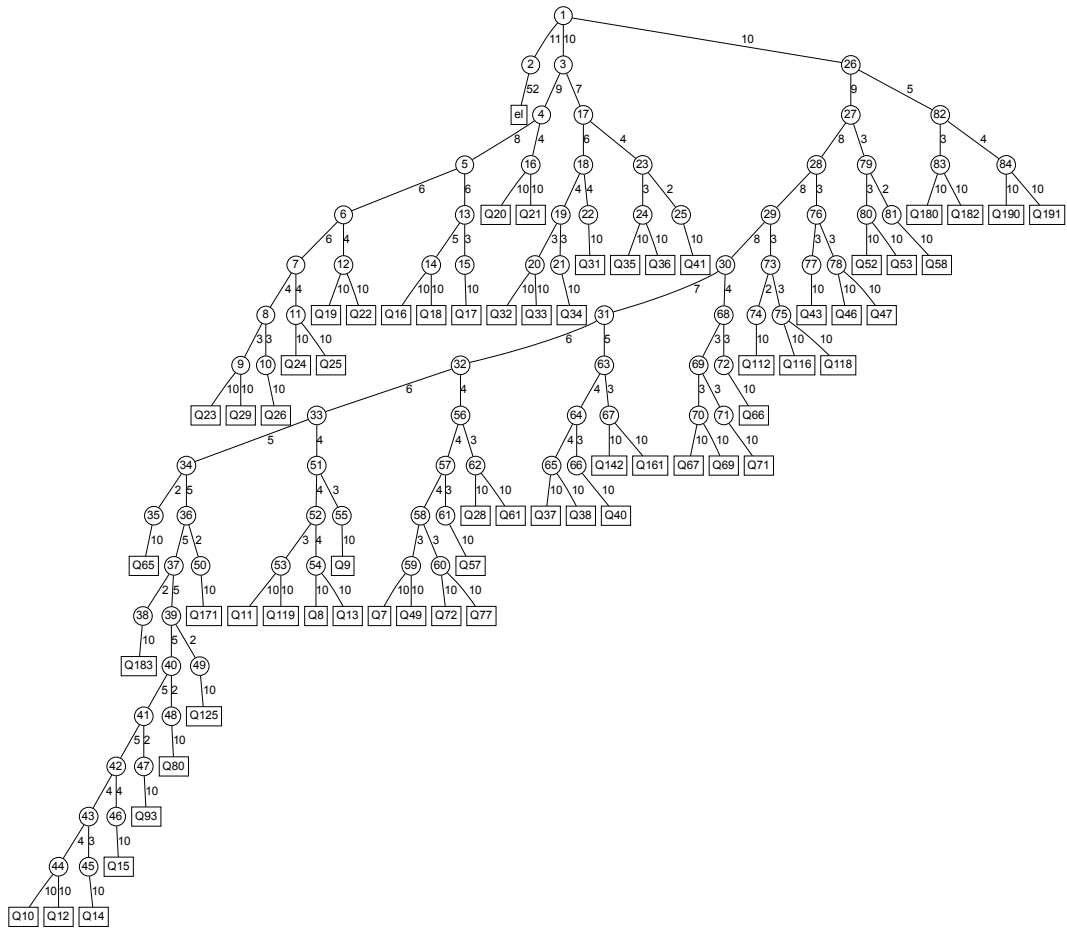


Figure S5: ML-tree for model (III).

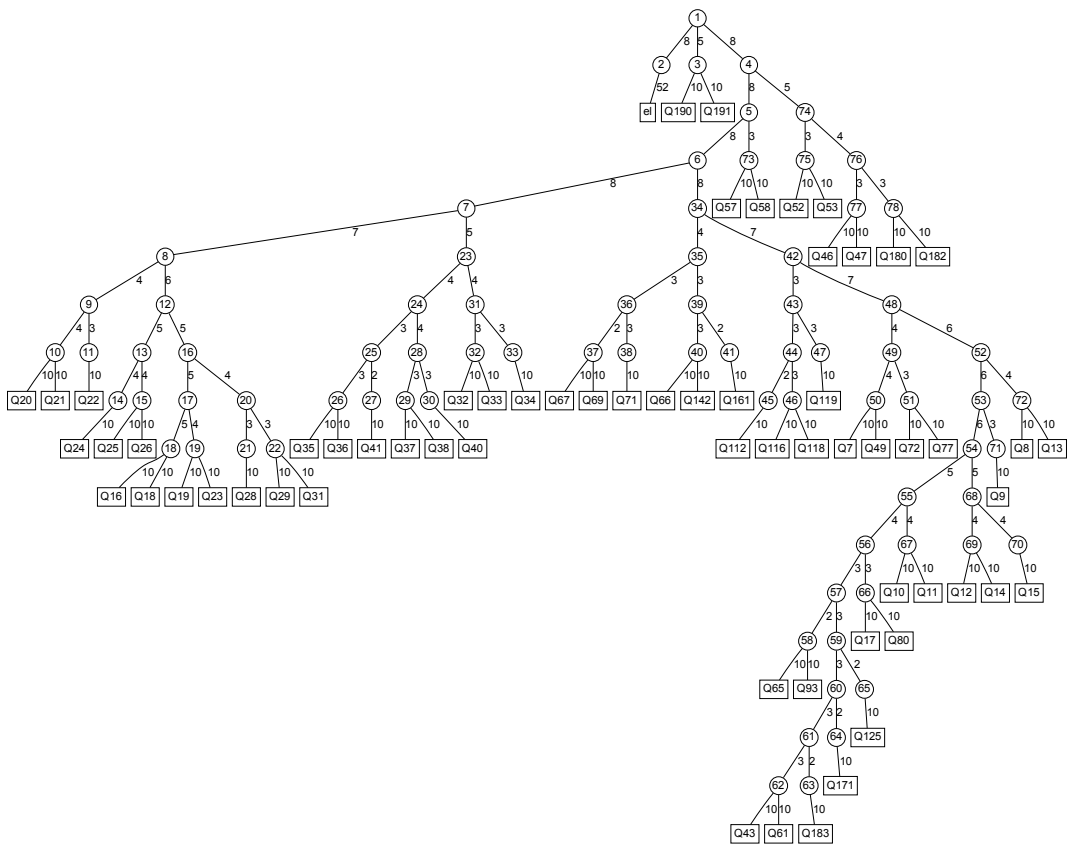


Figure S6: ML-tree for model (IV).

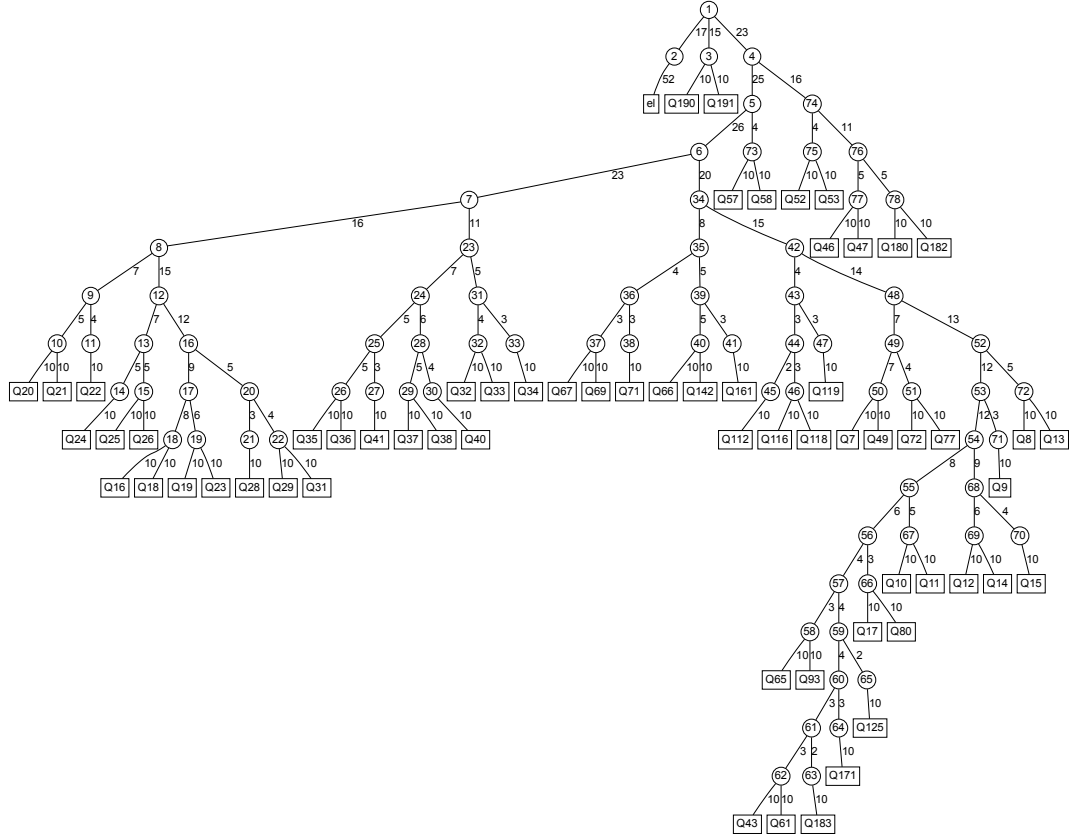


Figure S7: ML-tree for model (IV) and convergence of p_{NO} to 0.2%.

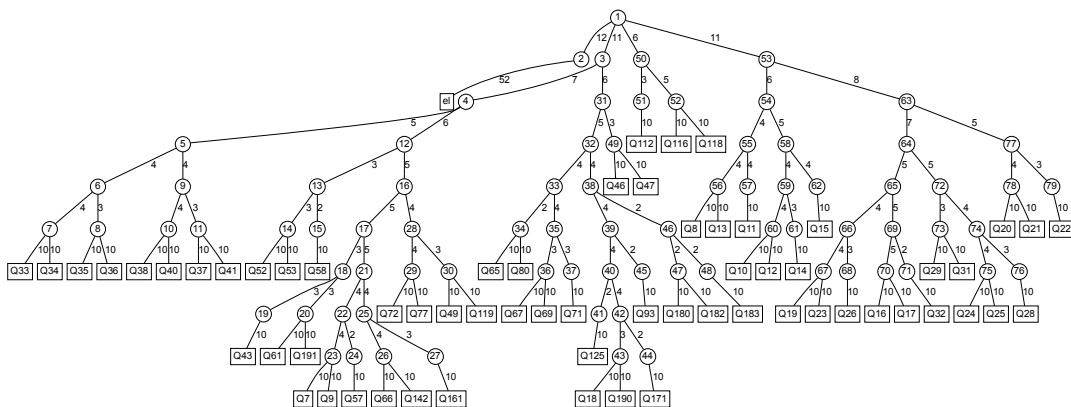


Figure S8: ML-tree for model (V).

S4 Adjacency Matrix of Model (IV)

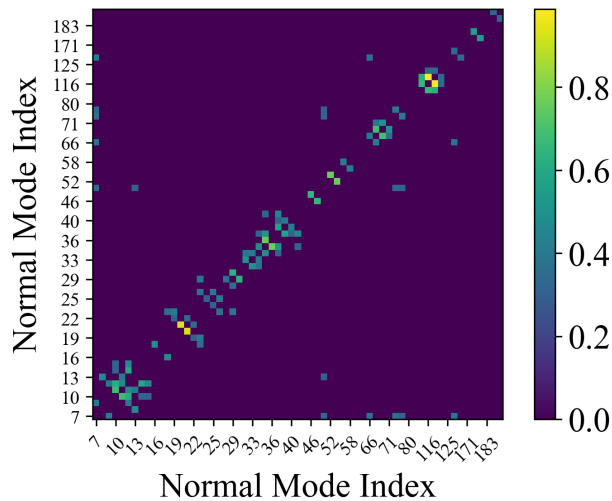


Figure S9: Adjacency matrix of model (IV), where a threshold of 0.3 has been used. A high threshold in the adjacency matrix results in most of the matrix elements taking the value 0.

S5 Population Dynamics for Larger Convergence Threshold

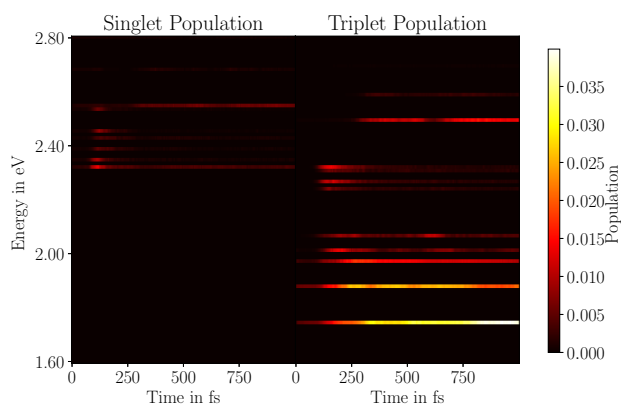


Figure S10: Time and energy resolved dynamics for model (I) with a threshold of $p_{\text{NO}} = 0.3\%$. Large shares of the population remain in the higher excited triplet states, which indicates that the computation is not sufficiently converged.

S6 42-dimensional Model

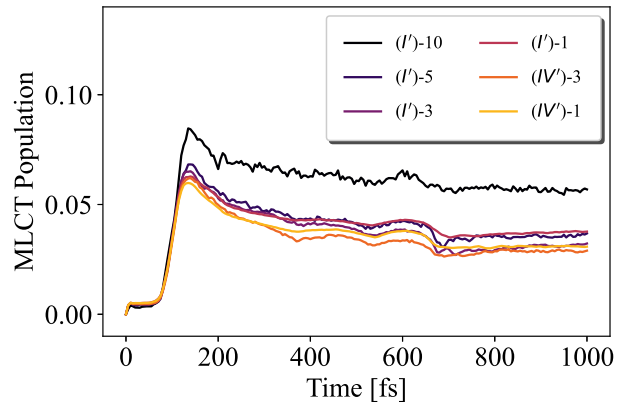


Figure S11: In order to check to what extent convergence with respect to p_{NO} can be achieved for different ML-trees with a reasonable computational effort, a smaller 42D model was studied. Setting the threshold for normal mode elongations in the TDH simulation to 0.2, a 42-dimensional model could be identified. Here, the cases with an adjacency matrix threshold of 0 (I') and 0.3 (IV') were considered. The figure shows population dynamics for the two models and different p_{NO} . Both cases converge to a rather similar limit. Looking at case (I') we notice that convergence is not monotonic. To improve convergence, p_{NO} would have to be reduced further, probably substantially.

S7 Discussion of Accuracy of State Couplings

A side aspect of the population dynamics is the slight increase in the MLCT population at the beginning of the simulation, which is present in all the computations (see Fig. 9 in the main text). For such early times, the laser field is still too weak to excite the system appreciably. Thus, the slight increase might indicate that the ground state geometry found through the quantum chemical geometry optimization on the adiabatic surfaces does not fully coincide with the minimum-energy ground state wave function including nonadiabatic couplings.

These small mixing between the diabatic ground state and the excited states arises from some small, non-zero λ parameters between the ground state and the excited states. The largest one of these λ parameters has a magnitude of about 0.041 eV (mode 148). These non-zero parameters with the ground state and their magnitude can have several origins. First, the λ parameters depend on the wave function overlap truncation threshold, but changing it from 0.998 to 0.99999 did not result in a significant change of the ground state-excited state λ values. Second, the parameters might exhibit a dependency on the stepsize (0.05 au) for the finite difference computation in Eqs. (7-8).¹ Ideally, the convergence with respect to the stepsize should be checked for each mode, but we did not undertake such a convergence study in the present work. Finally, an alternative origin for the non-zero ground state-excited state λ values could be the fact that, as a single-reference method that treats the ground and excited states on unequal footing, BSE@GW might not produce fully correct λ parameters for the ground state through the employed parametrization method. As the effect on the dynamics is small and it does not interfere with our goal, i.e., the exploration of spectral clustering for ML-tree generation, we postponed a more detailed exploration of this point to a future study.

S8 Dependence on the Used XC-Functional

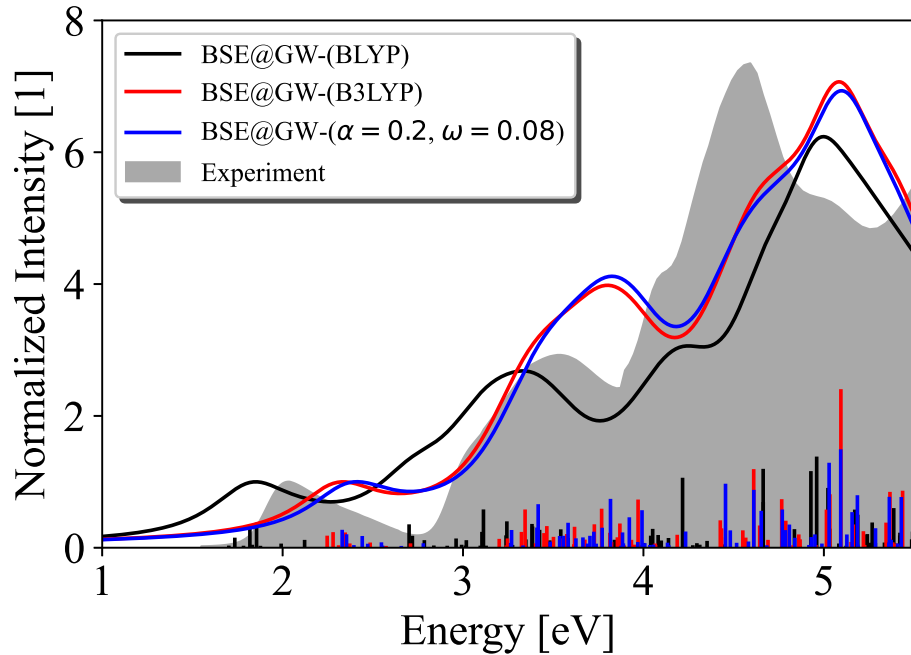


Figure S12: BSE@GW absorption spectra using the BLYP, B3LYP, and LC-BLYP functionals. The gray-shaded area refers to the experimental data from Refs. 2. One notices that including exact exchange removes the starting point dependence of BSE@GW. In contrast to earlier results on similar compounds the difference between BLYP and B3LYP is more pronounced.³

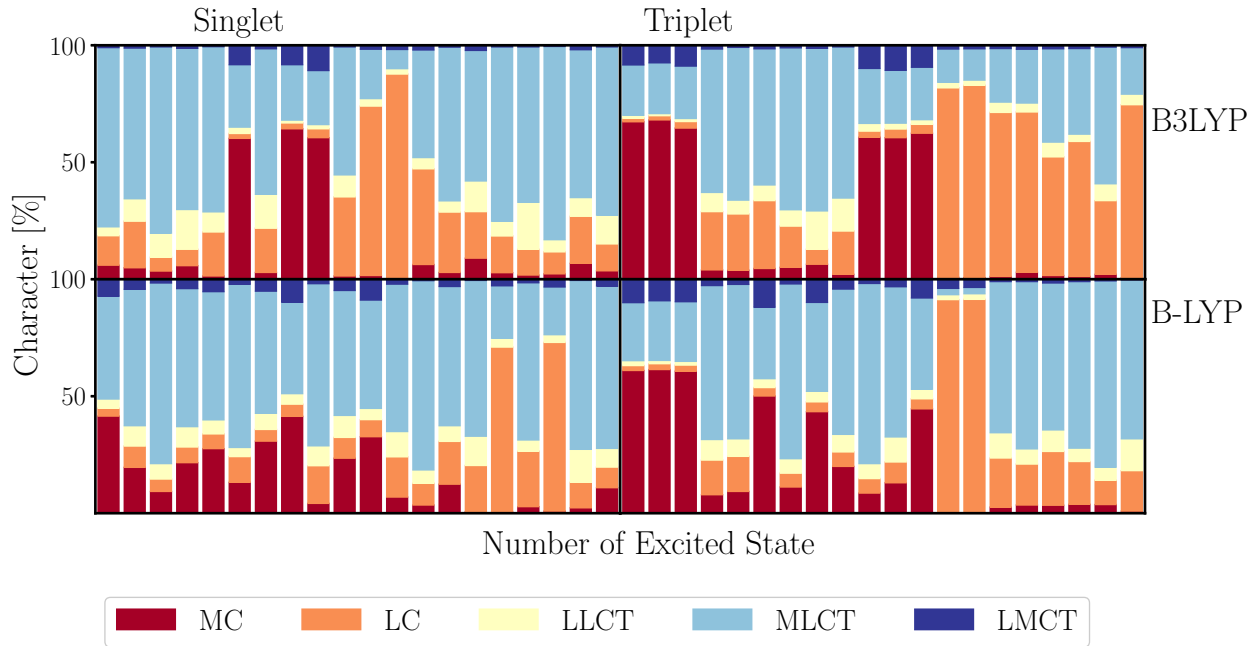


Figure S13: Analysis of the singlet and triplet TDM for the TDDFT transitions using the BLYP and B3LYP functionals. The absorption spectra are given in Fig. S12. We notice that the general pattern for MC and MLCT character is rather similar to LC-BLYP results in Fig. 4. The same holds true for the triplet transitions in case of BLYP. The deviations are more pronounced for the singlet BLYP case, in accordance with the difference in absorption spectra.

S9 Excitation Spectra

Table S1: Lowest Singlet States.

Level of Theory	State Index	Transition Energy [eV]	Oscillator Strength (len.) [a.u.]
$\alpha = 0, \omega = 0.14$	1	1.90930	0.00216
	2	1.94573	0.00062
	3	1.98022	0.03304
	4	2.00887	0.00033
	5	2.11412	0.04446
	6	2.30589	0.01092
	7	2.49610	0.00017
	8	2.64652	0.00119
	9	2.66425	0.00185
	10	2.93625	0.00854
	11	2.95663	0.02082
	12	2.99204	0.00307
	13	3.01781	0.00705
	14	3.04919	0.00368
	15	3.06392	0.00117
	16	3.09227	0.00540
	17	3.12763	0.00011
	18	3.13632	0.00067
	19	3.14477	0.00929
	20	3.15525	0.02363
$\alpha = 0.1, \omega = 0.11$	1	2.20340	0.00290
	2	2.23422	0.04381

Level of Theory	State Index	Transition Energy	Oscillator Strength
	3	2.24877	0.00242
	4	2.30140	0.00097
	5	2.36993	0.01488
	6	2.38106	0.00755
	7	2.49965	0.00588
	8	2.53356	0.00210
	9	2.58102	0.00427
	10	3.13353	0.01417
	11	3.13767	0.00869
	12	3.21643	0.00318
	13	3.22244	0.00669
	14	3.23630	0.02820
	15	3.25964	0.00850
	16	3.27789	0.00891
	17	3.29251	0.00110
	18	3.32457	0.00161
	19	3.38609	0.01015
	20	3.39602	0.00133
$\alpha = 0.15, \omega = 0.09$	1	2.31026	0.00005
	2	2.35094	0.01190
	3	2.38835	0.03040
	4	2.42410	0.00065
	5	2.44111	0.00022
	6	2.48407	0.01199
	7	2.50183	0.00546

Level of Theory	State Index	Transition Energy	Oscillator Strength
	8	2.55131	0.01282
	9	2.72882	0.00708
	10	3.20477	0.00380
	11	3.21217	0.00976
	12	3.27218	0.00670
	13	3.27446	0.02666
	14	3.29008	0.01055
	15	3.29207	0.00660
	16	3.40607	0.01965
	17	3.42674	0.00000
	18	3.47132	0.00001
	19	3.52854	0.01458
	20	3.53129	0.00133
$\alpha = 0.2, \omega = 0.08$	1	2.24621	0.00002
	2	2.36460	0.00097
	3	2.38761	0.00006
	4	2.61681	0.01402
	5	2.63450	0.04160
	6	2.65368	0.00001
	7	2.75380	0.00823
	8	2.81032	0.00686
	9	2.97645	0.00509
	10	3.27315	0.00130
	11	3.30519	0.00759
	12	3.36371	0.00912

Level of Theory	State Index	Transition Energy	Oscillator Strength
	13	3.37216	0.03646
	14	3.40490	0.00759
	15	3.41935	0.00035
	16	3.50583	0.00000
	17	3.63365	0.02638
	18	3.63579	0.00415
	19	3.64725	0.02309
	20	3.75438	0.00050
BSE@evGW	1	2.33014	0.03054
	2	2.35426	0.02201
	3	2.39508	0.00147
	4	2.44140	0.01880
	5	2.47188	0.00410
	6	2.54768	0.00677
	7	2.55399	0.00058
	8	2.65789	0.00001
	9	2.77995	0.00498
	10	3.26410	0.00566
	11	3.26647	0.00498
	12	3.26904	0.03018
	13	3.33288	0.00089
	14	3.40968	0.03484
	15	3.41653	0.07912
	16	3.48299	0.00822
	17	3.53556	0.01874

Level of Theory	State Index	Transition Energy	Oscillator Strength
	18	3.55651	0.01919
	19	3.58230	0.04387
	20	3.62586	0.01435

Table S2: Lowest Triplet States.

Level of Theory	State Index	Transition Energy [eV]	Oscillator Strength (len.) [a.u.]
$\alpha = 0, \omega = 0.14$	1	1.69681	0.01687
	2	1.77144	0.20949
	3	1.84538	0.02475
	4	1.85166	0.00470
	5	1.85896	0.00043
	6	1.91646	0.00639
	7	1.94470	0.01935
	8	1.98193	0.00690
	9	1.98536	0.00001
	10	2.10829	0.00004
	11	2.15793	0.01379
	12	2.22565	0.00048
	13	2.69512	0.15013
	14	2.69572	0.01910
	15	2.82394	0.18783
	16	2.85365	0.00011
	17	2.87666	0.07697
	18	2.92263	0.22047

Level of Theory	State Index	Transition Energy	Oscillator Strength
	19	2.94986	0.08752
	20	2.98771	0.00385
$\alpha = 0.1, \omega = 0.11$	1	1.68233	0.00020
	2	1.79961	0.00014
	3	1.80976	0.00151
	4	1.92221	0.00953
	5	1.95988	0.05028
	6	1.96972	0.00203
	7	2.06111	0.00242
	8	2.09160	0.14254
	9	2.13662	0.05161
	10	2.22015	0.00955
	11	2.24143	0.01918
	12	2.32303	0.00404
	13	2.76870	0.01852
	14	2.77041	0.17199
	15	3.05054	0.32750
	16	3.07690	0.00544
	17	3.12902	0.15634
	18	3.13472	0.00775
	19	3.15284	0.11679
	20	3.18834	0.07007
$\alpha = 0.15, \omega = 0.09$	1	1.59292	0.00013
	2	1.71153	0.00005
	3	1.72239	0.00061

Level of Theory	State Index	Transition Energy	Oscillator Strength
	4	1.91872	0.00006
	5	1.92524	0.00462
	6	2.01483	0.00004
	7	2.08255	0.00986
	8	2.24084	0.21044
	9	2.30396	0.03821
	10	2.39961	0.01505
	11	2.43214	0.01461
	12	2.53866	0.00240
	13	2.81104	0.01845
	14	2.81341	0.18441
	15	3.10953	0.00142
	16	3.11321	0.35874
	17	3.22340	0.01592
	18	3.24390	0.00557
	19	3.25444	0.17320
	20	3.30697	0.03063
$\alpha = 0.2, \omega = 0.08$	1	1.50116	0.00008
	2	1.62044	0.00001
	3	1.62887	0.00029
	4	1.86894	0.00004
	5	1.87636	0.00066
	6	1.96687	0.00002
	7	2.31104	0.00738
	8	2.47682	0.23059

Level of Theory	State Index	Transition Energy	Oscillator Strength
	9	2.54556	0.05450
	10	2.65404	0.02049
	11	2.70356	0.00700
	12	2.81468	0.00001
	13	2.88994	0.17147
	14	2.90054	0.01707
	15	3.18787	0.37464
	16	3.18854	0.00067
	17	3.36079	0.06109
	18	3.36362	0.00956
	19	3.43547	0.08815
	20	3.49872	0.04563
BSE@evGW	1	1.75339	0.00006
	2	1.84968	0.00017
	3	1.96999	0.00178
	4	2.02696	0.00645
	5	2.08566	0.16684
	6	2.25235	0.16250
	7	2.27567	0.02303
	8	2.32179	0.05756
	9	2.34079	0.00581
	10	2.47664	0.01088
	11	2.48619	0.00007
	12	2.56668	0.00164
	13	2.71941	0.04672

Level of Theory	State Index	Transition Energy	Oscillator Strength
	14	2.72069	0.00666
	15	2.81014	0.29784
	16	2.82558	0.03395
	17	2.96908	0.92086
	18	3.00414	0.03747
	19	3.11288	0.00463
	20	3.14112	0.01669

References

- (1) Farkhutdinova, D.; Polonius, S.; Karrer, P.; Mai, S.; González, L. Parametrization of Linear Vibronic Coupling Models for Degenerate Electronic States. *J. Phys. Chem. A* **2025**, *129*, 2655–2666.
- (2) Moll, J.; Naumann, R.; Sorge, L.; Förster, C.; Gessner, N.; Burkhardt, L.; Ugur, N.; Nuernberger, P.; Seidel, W.; Ramanan, C.; Bauer, M.; Heinze, K. Pseudo-Octahedral Iron(II) Complexes with Near-Degenerate Charge Transfer and Ligand Field States at the Franck-Condon Geometry. *Chemistry – A European Journal* **2022**, *28*, e202201858.
- (3) Bogdain, F.; Kühn, O. Performance of the Bethe–Salpeter Equation for Electronic Excitations in First-Row Transition Metal Complexes. *Journal of Chemical Theory and Computation* **2025**, *21*, 4494.